Structural Transition of Lamella Crystals in a Isomorphous Copolymer, Poly(3-hydroxybutyrate-*co*-3-hydroxyvalerate)

Naoko Yoshie,* Miwa Saito, and Yoshio Inoue

Department of Biomolecular Engineering, Tokyo Institute of Technology, 4259 Nagatsuta, Midori-ku, Yokohama 226-8501, Japan

Received July 23, 2001; Revised Manuscript Received October 6, 2001

ABSTRACT: The structure of the isomorphous crystals of P(HB-*co*-HV) in the PHB crystalline lattice is examined in detail, and a structural transition at ca. 10 mol % HV is found for the first time. By analyzing a series of P(HB-*co*-HV) samples prepared by the same treatment, the effect of the thermal history was removed from the results, and the composition dependence of the crystal formation and of the resultant crystalline structure was highlighted. The crystallinity, unit cell dimensions, and lamella thickness of P(HB-*co*-HV) were determined by X-ray analysis. The HV content in the crystalline phase was determined by high-resolution solid-state ^{13}C NMR spectroscopy. The thermal properties were studied by DSC. The crystallization kinetics was analyzed through the measurement of spherulite growth rate. It has been shown that the composition dependence of spherulite growth rate, crystallinity, lamella thickness, HV content in the crystalline phase, and melting temperature change discontinuously at ca. 10 mol % HV, indicating the occurrence of a structural transition at this composition. To explain these results, we have introduced two models of lamellar crystals containing counits, i.e., sandwich lamella and uniform lamella. We have concluded that P(HB-*co*-HV) with HV content below and above 10 mol % can be described by the sandwich lamella model the uniform lamella model, respectively.

Introduction

The crystalline state of a random copolymer lies between the two extremes, i.e., the crystals of complete comonomer exclusion and of complete comonomer inclusion.[1] The former crystal is composed entirely of A units, while the comonomer composition of the latter crystal equals to the whole composition of the copolymer. Thus, the content of B counits in the crystalline phase, f_B^c, is $0 \le f_B^c \le f_B$, where f_B is the B content of the whole copolymer. In most copolymer systems, the excess free energy upon the inclusion of a B unit into the A crystalline lattice is large compared with the free energy of fusion of an A unit at any crystallization temperature. So, the content of B units in the crystalline phase is near zero. There are a few systems where the content of B units in the A crystalline lattice is quite large (though is smaller than f_B). Such a crystalline state is called isomorphism. Poly(3-hydroxybutyrate-*co*-3-hydroxyvalerate) (P(HB-*co*-HV)) is one of the well-studied examples of isomorphous copolymers.

P(HB-*co*-HV) is well-known as a biodegradable thermoplastic material produced by bacterial fermentation. In previous studies,[2−5] several evidences of isomorphism in P(HB-*co*-HV) have been found by using wide-angle X-ray diffraction, solid-state NMR spectroscopy, differential scanning calorimetry, and polarized microscopy. A high-level crystallinity is preserved at all compositions between 0 and 95 mol % HV. The crystalline phase developed in P(HB-*co*-HV) transforms from the PHB lattice to the PHV lattice at ca. 50 mol % HV. At the same composition, the melting temperature takes the minimum value. The composition dependence of the spherulite growth rate also reaches the minimum at ca. 50 mol % HV. All of these observations are keeping with the hypothesis of isodimorphism;[2] i.e., HV units are partially included in the PHB lattice and HB units are partially included in the PHV lattice. The HV content of the crystals in the PHB lattice has been determined by using high-resolution solid-state ^{13}C NMR spectroscopy,[6,7] wide-angle X-ray diffraction analysis,[8,9] and density measurement.[10] Though these studies also supported the hypothesis of isomorphism, they failed to reach agreement on the amount of HV units in the PHB lattice. The amount varied from 30%[6] to 100%[9] of the total HV content in the copolymer. This variation is probably ascribed to the fact that each research group used different P(HB-*co*-HV) samples of various comonomer composition prepared by various thermal treatment. In fact, it has been reported that the composition in the crystalline phase of P(HB-*co*-HV) changes depending on the crystallization temperature.[11,12]

In this study, we have reexamined the structure of the isomorphous crystals of P(HB-*co*-HV) with 0−29 mol % HV. In this composition range, HV units cocrystallize with HB units in the PHB lattice. By analyzing a series of P(HB-*co*-HV) samples prepared by the same treatment, the effect of thermal history was removed from the results, and the composition dependence of the crystallization and of the resultant structure was highlighted. The crystallinity, unit cell dimensions, long period, and lamella thickness of P(HB-*co*-HV) were determined by X-ray analysis. The HV content in the crystalline phase was determined by high-resolution solid-state ^{13}C NMR spectroscopy. The thermal properties were studied by DSC. The crystallization kinetics was analyzed through the measurement of spherulite growth rate. The results of these analyses have indicated the occurrence of a structural transition at ca. 10 mol % HV. This type of transition had not been reported in previous reports. To explain this transition, we have introduced two models of lamellar crystals containing counits, i.e., sandwich lamella and uniform lamella.

* To whom correspondence should be addressed. E-mail: nyoshie@bio.titech.ac.jp.

10.1021/ma0113071 CCC: $20.00
Published on Web 11/22/2001

Table 1. Molecular Characteristics of PHB and P(HB-*co*-HV)

polyester	HV content[b]/%	$M_w \times 10^{-5}$ [c]	M_w/M_n[c]	^{13}C content in methine[d]/%
PHB^N	0	6.0	2.4	1.1[e]
P(HB-*co*-6% HV)^E	5.9	7.9	2.4	11.9
P(HB-*co*-9% HV)^E	9.1	7.9	2.7	9.7
P(HB-*co*-9% HV)^N	9.2	7.2	2.7	1.1[e]
P(HB-*co*-13% HV)^E	12.9	4.4	2.7	11.7
P(HB-*co*-15% HV)^N	15.1	4.6	1.5	1.1[e]
P(HB-*co*-21% HV)^N	21.0	7.1	2.3	1.1[e]
P(HB-*co*-29% HV)^N	28.8			1.1[e]

[a] Superscripts E and N indicate the samples with and without ^{13}C enrichment, respectively. [b] Measured by ^1H NMR. [c] Measured by GPC. [d] Measured by ^1H-coupled ^{13}C NMR. [e] Natural abundance of ^{13}C.

Experimental Section

Materials. When the composition in the crystalline phase of P(HB-*co*-HV) with low HV content is determined by the curve decomposition of solid-state ^{13}C NMR spectra, the P(HB-*co*-HV) sample containing a natural abundance of ^{13}C often gives rise to large experimental error because the peak intensity of HV resonance is much smaller than that of HB resonance. To make the apparent intensity of HV resonance comparable to that of HB resonance, P(HB-*co*-HV) samples of which HV units were labeled with ^{13}C were prepared.

Samples of P(HB-*co*-HV) were prepared by a two-stage fermentation procedure of *Ralstonia eutropha* H16 (ATCC17699) as previously reported.[13] This involves the stages for bacterium growth and for polyester accumulation. The carbon sources used for the polyester accumulation were mixtures of acetic and propionic acids. Polyesters were extracted from the dried cells with hot chloroform and purified by reprecipitation with hexane. Labeled samples of P(HB-*co*-HV) were produced from mixtures of natural acetic acid and [1-^{13}C]propionic acid (^{13}C content ≈ 10 mol %). When a carbon source containing [1-^{13}C]-propionate is used, the methine carbon of HV units is labeled with ^{13}C.[13] When we need to discriminate the P(HB-*co*-HV) samples with and without ^{13}C label explicitly, we denote them as P(HB-*co*-HV)^E and P(HB-*co*-HV)^N, respectively. In previous papers,[14−16] it has been reported that bacterial copolyesters often have very broad and/or polymodal chemical composition distribution. So, the samples isolated from bacteria were subjected to the compositional fractionation by using the chloroform/heptane mixed solvent. Details of the fractionation were described elsewhere.[14] Four P(HB-*co*-HV)^N fractions (HV content 9, 15, 21, and 29 mol %) and three P(HB-*co*-HV)^E fractions (HV content 6, 9, and 13 mol %), in addition to PHB of natural abundance (PHB^N), were used in this study.

Melt-crystallized samples were prepared by the compression-molding process performed on a Toyoseiki Mini Test Press-10. The samples were inserted between aluminum plates with an aluminum spacer (0.1 mm thickness) and were compression-molded at 195 °C for 3 min under a pressure of 5 MPa. The molten samples were then cooling to 90 °C and kept for 4 weeks to reach the equilibrium crystallinity prior to the analysis. It is known that P(HB-*co*-HV) copolymers are thermally unstable at temperatures above 170 °C. The rate of chain scission is, however, independent of the comonomer compositions.[17] Thermal degradation cannot bias the discussion of this study concerning on the composition dependence of the various structural parameters.

Molecular characteristics of PHB^N, P(HB-*co*-HV)^N, and P(HB-*co*-HV)^E samples are listed in Table 1. Molecular weights, HV contents, and ^{13}C contents in the HV methine position of P(HB-*co*-HV)^E samples were determined by GPC, solution-state ^1H NMR spectroscopy, and solution-state ^1H-coupled ^{13}C NMR spectroscopy, respectively, as previously reported.[18] The ^{13}C contents in the methine position of HV units were determined to be ≈10 mol %. From the data on the ^{13}C content, the ^{13}C content in the whole P(HB-*co*-HV)^E samples was estimate to be less than 1.4%, which is not so different from the natural abundance. We can assume that ^{13}C enrichment has no effect on the physical properties of P(HB-*co*-HV)^E samples.

Structural Analysis. Wide-angle X-ray diffraction (WAXD) and small-angle X-ray scattering (SAXS) measurements were made on a Rigaku RU-200 operated at 50 kV and 180 mA. Nickel-filtered Cu Kα radiation ($\lambda = 0.154$ nm) was used. WAXD patterns were recorded in the 2θ range 5−50° at a scan speed of 1.0°/min at room temperature. Assuming that the diffraction peaks from a crystallographic plane and the amorphous halo could be reproduced by a Gaussian curve and a sum of two Gaussian curves, respectively, diffraction patterns in the 2θ range 5−33° were resolved into a series of Gaussian peaks by curve-fitting using the damped least-squares algorithm. The degree of crystallinity (χ_{waxd}) was calculated from the relative areas of the resolved peaks. SAXS patterns were recorded in the 2θ range 0.1−2.5°. Each step increased 2θ by 0.004°, and X-rays were collected for 4 s at each step. The long period was determined from the local maximum of the one-dimensional correlation function.

High-resolution solid-state ^{13}C NMR spectra were recorded at 100 MHz on a Varian Unity-400 NMR spectrometer equipped with CPMAS accessories. ^{13}C CPMAS NMR spectra were acquired with a 5 s pulse repetition, a 50 kHz spectral width, 4K data points, and 1200−4000 accumulations under high-power ^1H decoupling. The contact time was 2 ms, and the MAS rate was 4.0 kHz. The methine carbon resonance was resolved into four Lorenzian curves by a curve-fitting procedure using the damped least-squares algorithm. The decomposed curves were assigned to the resonances from the HB units in the crystalline phase, the HB units in the amorphous phase, the HV units in the crystalline phase, and the HV units in the amorphous phase.[6] The comonomer composition in the crystalline phase was calculated from the ratio of the peak areas due to the HB and HV units in the crystalline phase.

Thermal Analysis. Thermal characterization was conducted on a Seiko EXSTAR6000 system equipped with a DSC 220U. Melt-pressed films of 3−6 mg were encapsulated in aluminum pans and heated from room temperature to 200 °C at a heating rate of 20 °C/min. The melting temperature was taken as the peak top.

Spherulite growth rates were measured by polarized microscopy. Analysis was carried out with an Olympus BX 90 polarized microscope equipped with a Mettler FP82HT hot stage. Film samples were heated to 195 °C, kept at this temperature for 1 min, and then cooled to a selected crystallization temperature where they were kept isothermally. The spherulite growth rate was taken as the slope of the linear plot of spherulite radius vs time.

Results

Analysis of Spherulite Growth Rate. To analyze the crystallization kinetics, the spherulite growth rate, *G*, of the P(HB-*co*-HV) samples was measured at temperatures between 60 and 110 °C. Log *G* of each sample is plotted as a function of crystallization temperature in Figure 1a. The plots show the trend similar to the results reported in previous papers.[4,19] For the composition range from 0 to 21 mol % HV, the growth rate markedly decreases, and the whole rate curve moves to lower temperature as HV content increases.

To examine the composition dependence of the crystallization kinetics further, log *G* at each crystallization temperature is replotted as a function of HV content in Figure 1b. Noticeable feature of this figure is that the slope of the plots changes at ca. 10 mol % HV at any crystallization temperature between 60 and 110 °C. While the data in the composition ranges between 0 and 10 mol % HV and between 10 and 21 mol % HV give linear plots, the slope of the former range is much smaller than that of the latter. This implies that the crystallization kinetics changes at ca. 10 mol % HV.

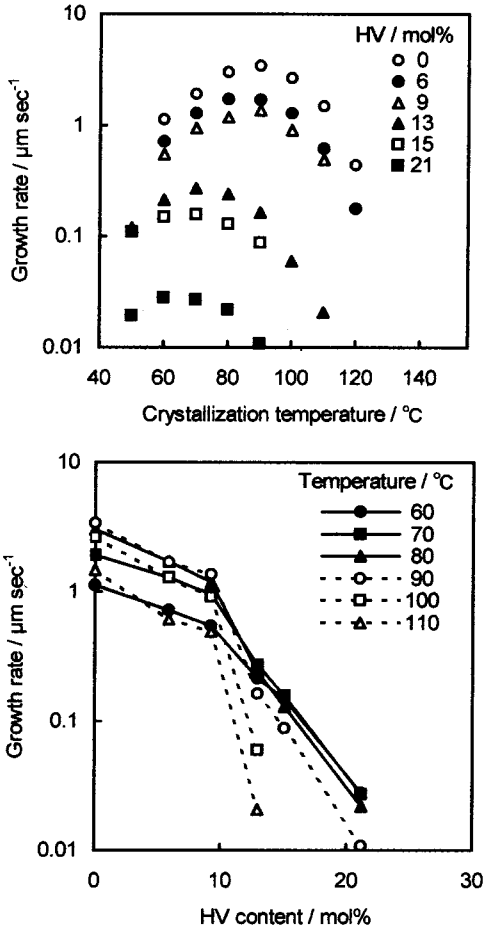

Figure 1. (a) Spherulite growth rate of P(HB-*co*-HV) containing 0−21 mol % HV as a function of crystallization temperature. (b) Spherulite growth rate at 60−110 °C as a function of HV content.

Spherulite growth kinetics is often analyzed by using a secondary nucleation model proposed by Hoffman.[20] This excellent model directs toward the analysis of the spherulite growth of homopolymers and copolymers that do not exhibit cocrystallization. So, it does not consider the case of cocrystallization where the thermal history may affect the comonomer composition in the crystalline phase. It has been reported that the composition in the crystalline phase of P(HB-*co*-HV) varies depending on the crystallization temperature.[11,12] The secondary nucleation model is not applicable to the case of P(HB-*co*-HV). For further consideration of the change in the crystallization kinetics at ca. 10 mol % HV of P(HB-*co*-HV), the samples crystallized at 90 °C were analyzed by WAXD, SAXS, solid-state NMR, and DSC.

X-ray Analysis of Crystal Structure. Figure 2 shows WAXD patterns of the P(HB-*co*-HV) samples containing 0−29 mol % HV. All of them correspond to the patterns given by the PHB crystalline lattice reported in previous papers.[21,22] No evidence of the existence of the PHV crystalline lattice was observed. It has been reported that P(HB-*co*-HV) crystallizes in either the PHB or PHV crystalline lattice for HV content lower or higher than 50 mol %.[2,5] Our result is consistent with these reports.

The diffraction patterns were resolved into the amorphous halo and the diffraction peaks from the crystalline phase. The degree of crystallinity, χ_{waxd}, was estimated from the relative areas of the resolved peaks. Figure 3

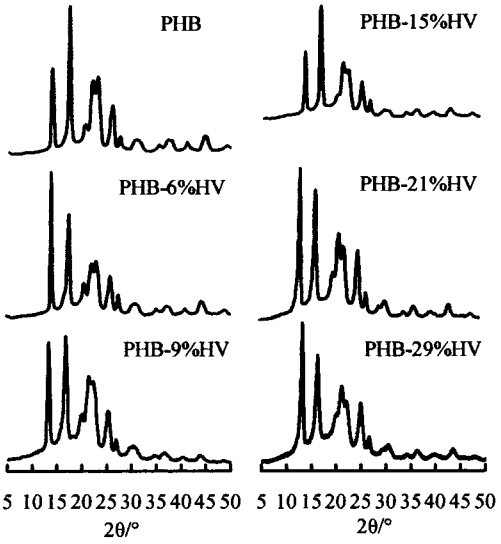

Figure 2. Wide-angle X-ray diffraction patterns of P(HB-*co*-HV) containing 0−29 mol % HV.

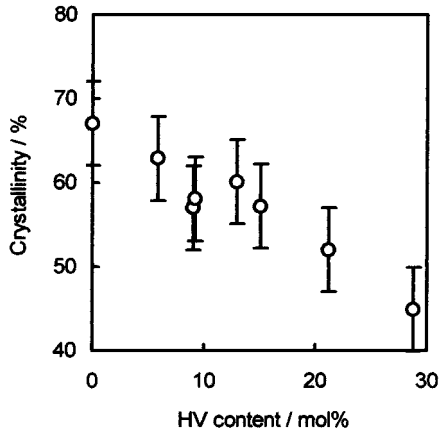

Figure 3. Degree of crystallinity of P(HB-*co*-HV) as a function of HV content.

shows the degree of crystallinity as a function of HV content. In agreement with previous reports,[2,3] a high level of crystallinity is kept at all compositions between 0 and 29 mol % HV. The high level crystallinity has been regarded as an evidence of the isomorphism.

Though the degree of crystallinity of our sample slightly decreased with increasing HV content, small fluctuation of the data was observed. The degree of crystallinity slightly increased at ca. 10 mol % HV. Though the amplitude of the fluctuation is not beyond the level of experimental error, it is notable that the fluctuation occurs just at the composition where the change in the crystallization kinetics is suggested by the analysis of spherulite growth rate. The fluctuation may be related to the change in the crystallization kinetics.

The *d* spacings determined from the peak positions of WAXD patterns are plotted as a function of HV content in Figure 4. With increasing HV content, an obvious expansion of *d*(110) spacing and a small expansion of *d*(020) spacing were observed, while *d*(002) spacing was kept constant. In previous papers,[23,24] the crystalline lattice expansion was interpreted as a consequence of comonomer inclusion. The side chain of HV units in the PHB crystalline lattice causes expansion in directions of the plane perpendicular to the chain axis (i.e., the *ab* plane).

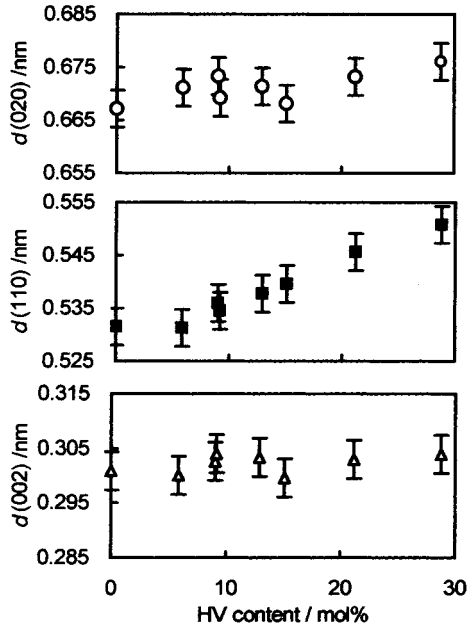

Figure 4. X-ray diffraction $d(020)$, $d(110)$, and $d(002)$ spacings of P(HB-*co*-HV) as a function of HV content.

When the plots of Figure 4 were carefully examined, it became clear that the slope of the plot of $d(110)$ spacing changed at ca. 6 mol % HV. The $d(110)$ spacing of P(HB-*co*-6% HV) is similar to that of PHB, while the spacing linearly increases in the composition range above 6 mol % HV. This observation suggests that the HV units are hardly included in the crystalline phase for P(HB-*co*-6% HV), while the HV units are partially included in the crystalline phase in the composition range above 6 mol % HV. The composition in the crystalline phase is quantitatively analyzed by solid-state ^{13}C NMR spectroscopy later.

The long period, L, of the samples was determined from the maximum of the first-order correlation function estimated from the SAXS patterns. Assuming a simple two-phase model of lamella morphology, lamella thickness, L_c, can be estimated by the product of L and the volume fraction of crystal, χ_v. Properly speaking, χ_v is not equal to the crystallinity determined from WAXD, χ_{waxd}. The volume fraction of crystal, χ_v, is calculated from the mass fraction of crystal, χ_m, by

$$\chi_v = \frac{\rho^a}{(1-\chi_w)\rho^c + \chi_w \rho^a}\chi_w \qquad (1)$$

where ρ^c and ρ^a are the crystalline and amorphous densities, respectively. We can safely assume that $\chi_m \approx \chi_{waxd}$ because the electron density is approximately proportional to the mass. The amorphous density, ρ^a, for P(HB-*co*-HV) is reported to be $1.178 - 0.067 f^a_{HV}$ g/cm^3, where f^a_{HV} indicates the mole fraction of HV units in the amorphous phase.[10] The crystalline density, ρ^c, for PHB[21] is 1.26 g/cm^3, and that of P(HB-*co*-HV) in PHB crystalline lattice is independent of the HV content in the crystalline phase.[25] Thus, the ratio of ρ^a to ρ^c is between 0.9 and 1.0 for P(HB-*co*-HV) containing 0−29 mol % HV. The difference between χ_v and χ_{waxd} is less than 0.015, which is much less than the experimental error of χ_{waxd}. Therefore, we have estimated lamella thickness, L_c, as a product of L and χ_{waxd} and thickness of the amorphous layer, L_a, as $L - L_c$.

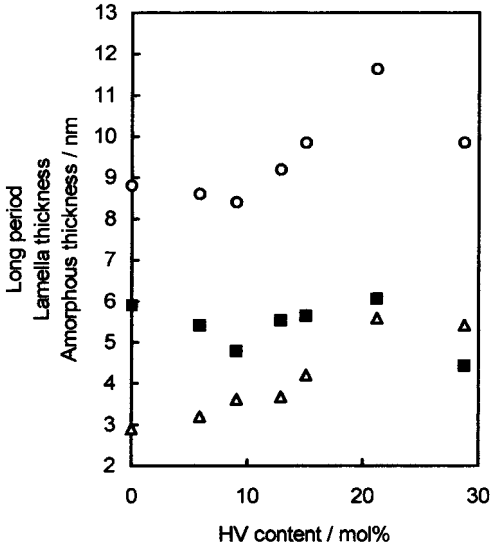

Figure 5. Long period (open circle), lamella thickness (closed square), and amorphous layer thickness (open triangle) of P(HB-*co*-HV) as a function of HV content.

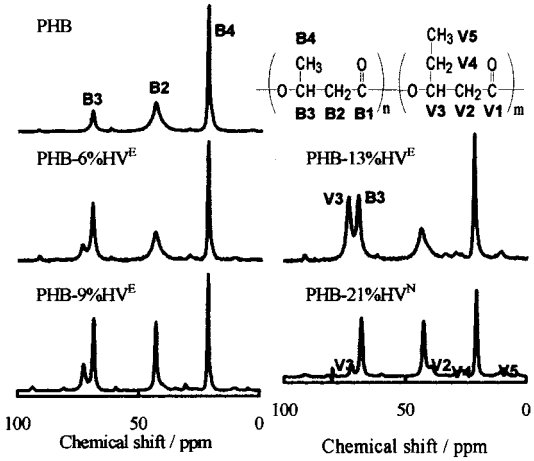

Figure 6. ^{13}C CPMAS NMR spectra of methyl, methylene, and methine regions for P(HB-*co*-HV) containing 0−21 mol % HV.

The data on L_c and L_a, together with L for the P(HB-*co*-HV) samples are plotted as a function of HV content in Figure 5. Though L_a gradually increases with HV content, L and L_c take minimum values again at 10 mol % HV. Though the minimum in the L_c vs HV content curve has also been observed in previous studies,[26,27] the origin of the minimum was not discussed. The L_c value takes minimum again at the composition where the change in the crystallization kinetics is suggested by the analysis of spherulite growth rate. This implies the change in the crystallization kinetics and in the resultant structure.

Solid-State NMR Analysis of the Composition in the Crystalline Phase. ^{13}C CPMAS NMR spectra of P(HB-*co*-HV) were measured to determine the composition in the crystalline phase. Figure 6 shows methyl, methylene, and methine resonances of ^{13}C CPMAS NMR spectra for the P(HB-*co*-HV) samples. The peak assignments are also shown in the figure. In the spectra of P(HB-*co*-6% HV)^E, P(HB-*co*-9% HV)^E, and P(HB-*co*-13% HV)^E, the V3 peak has a peak area comparable to the B3 peak because of the ^{13}C enrichment. We can expect this enrichment to reduce the experimental error in the curve decomposition procedure.

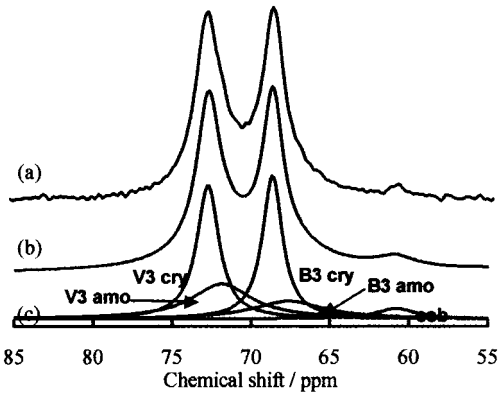

Figure 7. Experimental and calculated resonances from the methine carbons for P(HB-*co*-13% HV)^{E}: (a) experimental; (b) total curve of c; (c) simulated resonances. Ssb indicate spinning sideband.

Assuming a two-phase model, the methine (B3, V3) resonances were decomposed into four Lorenzian curves assigned to HB in the crystalline phase, HB in the amorphous phase, HV in the crystalline phase, and HV in the amorphous phase. For the peak assignment we were referred to previous papers.[6,7,18] Figure 7 shows experimental and calculated resonances from the methine carbons for P(HB-*co*-13% HV)^{E}. HV content in the crystalline phase, f_{HV}^{c}, was given by

$$f_{HV}^{c} = \frac{A_{V3}/E_{V3}r_{V3}}{A_{B3}E_{B3}r_{B3} + A_{V3}/E_{V3}r_{V3}} \qquad (2)$$

where A_i, E_i, and r_i are peak area of the resonance from i carbon in the crystalline phase, CP efficiency of i carbon, and ^{13}C population of i carbon, respectively. Here, the B3 carbon is in natural abundance, i.e., $r_{B3} = 0.011$. In general, the CP efficiency of each carbon species is different because the strength of the $^{1}H-^{13}C$ dipole interaction depends on the environments surrounding the carbon atoms of interest. However, the environment of the main-chain methine carbons, B3 and V3, in the crystalline phase of P(HB-*co*-HV) is similar because (1) HB and HV units cocrystallize in the PHB crystalline lattice, (2) the chemical structure of HB unit is similar to that of HV unit, and (3) the motion of the backbone carbons is limited in the crystalline region. Therefore, we could assume that the CP efficiencies of B3 and V3 carbons of P(HB-*co*-HV) are the same. Actually, this assumption was confirmed by the measurement of CPMAS NMR spectra taken with various proton spin-locking times prior to CP):[7] the spectra with different spin-locking times gave similar ratio of A_{V3} to A_{B3} for P(HB-*co*-21% HV).

The relation between the composition in the crystalline phases and the overall composition is shown in Figure 8. The solid line in the figure indicates the case where both of the crystalline and amorphous phases have the same composition. It was obvious that the HV content in the crystalline phase, f_{HV}^{c}, is smaller than the whole composition, f_{HV}, for P(HB-*co*-HV) containing 0−29 mol % HV. The data in Figure 8 show that the ratio of f_{HV}^{c} to f_{HV} changes. The ratios for the samples with lower and higher HV contents are one-half and two-thirds, respectively. It is noteworthy that the composition at which the ratio changes is again at ca. 10 mol % HV.

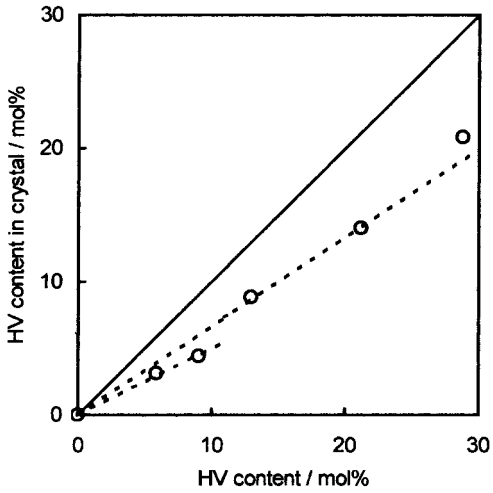

Figure 8. HV content in the crystalline phase as a function of overall HV content. The solid line indicates the case in which both of the crystalline and amorphous phases have the same composition. The broken lines indicate the cases where the HV content of the crystalline phase are one-half and two-thirds of the whole HV content.

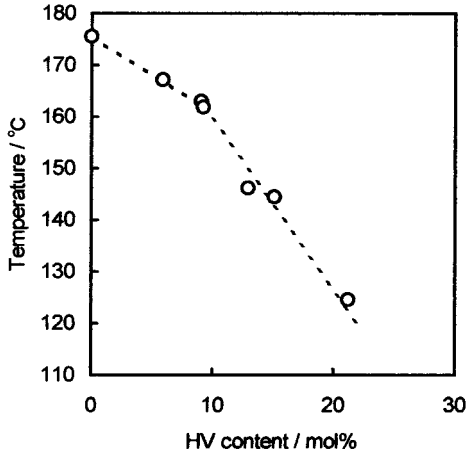

Figure 9. Melting temperature of P(HB-*co*-HV) containing 0−29 mol % HV as a function of HV content. The broken line is drawn as a guide only.

Thermal Analysis. Figure 9 shows the melting temperature for the samples as a function of HV content. In agreement with a previous paper,[2] the melting point is depressed as the HV content increases. The close observation of the figure indicates that the slope of the plot changes at ca. 10 mol % HV, once again. The slope for the composition range of 0−10 mol % HV is smaller than that for the range above 10 mol % HV.

Discussion

In the previous section, it has been shown that the composition dependence of spherulite growth rate, crystallinity, lamella thickness, HV content in the crystalline phase, and melting temperature change discontinuously at ca. 10 mol % HV. Although the discontinuity in some of these plots is not obviously beyond the experimental error, the point is that all the plots show the discontinuity at the same composition. Therefore, all of these results in coordination indicate a structural transition at this composition. To explain this transition, we introduce two models of lamellar crystals that include counits. Figure 10 is a schematic representation of the models. In the uniform lamella

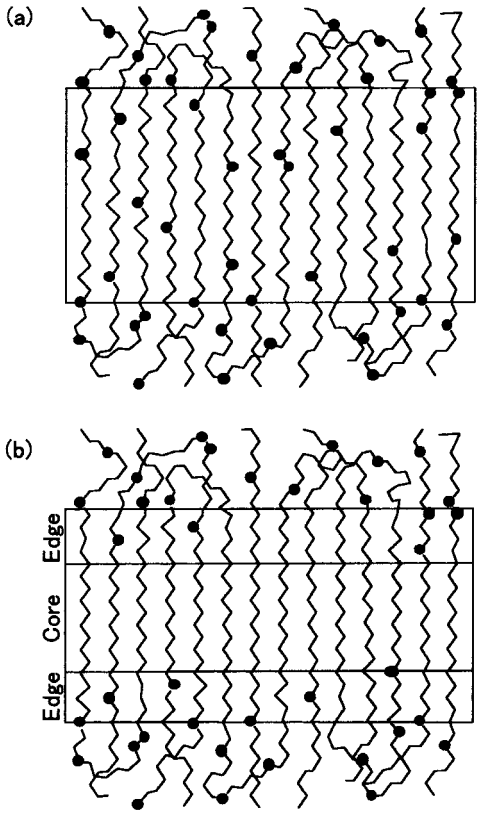

Figure 10. Schematic drawings of two models of lamellar crystals that include counits: (a) uniform lamella in which the counits are uniformly distributed in the lamella and (b) sandwich lamella in which the core is composed entirely of the major unit and the counits exist only in the edge of the lamella.

model, counits are uniformly distributed in the lamellar. The sandwich lamella model consists of edge parts and a core part between them. The core is composed entirely of the major units, and the counits exist only in the edges.

The free energy of formation of cocrystals is given by the sum of the free energy of the crystallization of the A homopolymer, the excess free energy and the configurational entropy upon the inclusion of B counits into the A lattice, and the surface free energy. The excess free energy of cocrystallization is usually positive though the absolute value must be small for the case of isomorphous copolymers like P(HB-*co*-HV). Therefore, in P(HB-*co*-HV) of low HV content where relatively long HB sequences are abundant and the entropy gain upon the cocrystallization is little, there must be a marked tendency for the HV units to be excluded from the lamella. Even if this is the case, the HV units may exist in the lamella surface where the distortion of the crystalline lattice upon the inclusion of the HV units can be easily relaxed. Therefore, the sandwich lamella model may better describe the isomorphism of P(HB-*co*-HV) with low HV content. In the sandwich lamella state the core thickness is expected to decrease with the increase of the HV content in the copolymer because the average length of the HB sequences decreases. Actually, as shown in Figure 5, L_c of P(HB-*co*-HV) has decreased with the increase of the HV content from 0 to 10 mol %.

The formation of sandwich lamella can gain advantage over the formation of uniform lamella only when the core is sufficiently thick. At a certain HV content where the core become thinner than a certain limit, stable sandwich lamella cannot be formed, and the uniform lamella model can better describe the crystalline state of P(HB-*co*-HV) samples. This content must be ca. 10 mol % HV. For the composition range from 10 to 21 mol % HV, the increase of L_c with the HV content was observed (see Figure 5). This can be ascribed to the change in the degree of supercooling. As is well-known, the melting temperature of P(HB-*co*-HV) decreases with the increase of the HV content at this composition range.[2] So, the degree of supercooling decreases with the HV content.

Figure 3 suggests that at ca. 10 mol % HV the sandwich lamella state has smaller crystallinity than the uniform lamella state. Since the core of the sandwich lamella is composed of only the HB units, the sequences that can participate in the crystalline lattice are limited to those having a long HB sequence in the center. On the other hand, the HV units can participate in any part of the uniform lamella. Therefore, the fractional population of the sequences those can participate to the uniform lamella is larger than the population of the sequences those can participate to the sandwich lamella. Figure 3 also shows that for both the sandwich lamella state and the uniform lamella state the crystallinity decrease with the increase of the HV content. This must be ascribed to the fact that the HV content in the crystalline state is one-half or two-thirds of the whole composition. The fractional population of the monomers that are excluded from the lamella increases with the HV content, f_{HV}, as $0.5f_{HV}$ or $0.33f_{HV}$.

The assumption of the transition form a sandwich lamella to a uniform lamella is also consistent with the data of *d* spacings (Figure 4) and melting temperature (Figure 9). Since the core of the sandwich lamella is free from the lattice defect of HV units, the lattice dimensions and the melting temperature of the core are similar to those of PHB. For a sandwich lamella state, the *d* spacing determined from the peak top of the WAXD patterns must represent the lattice dimensions of the core because the crystalline lattice of the core is more ordered than that of the edge. The disordered lattice of the edge must contribute to the broadening of the peak. Thus, the result that the *d* spacings of P(HB-*co*-6% HV) determined by WAXD was similar to those of PHB (see Figure 4) is consistent with the sandwich lamella model. The apparent melting temperature of a sandwich lamella must be similar to the melting temperature of the core because up to this temperature the unmelted core restricts the mobility of the molecules in the edges even if the edges melt at a lower temperature. Thus, the result that the melting temperature of P(HB-*co*-HV) containing less than 10 mol % HV was as high as that of PHB (see Figure 9) is also consistent with the sandwich lamella model. For the HV content above 10 mol % HV, it was observed that the *d*(110) spacing increases and the melting temperature decreases as the HV content increases. These results are consistent with the uniform lamella model where the HV content increases with the HV content of the whole copolymer.

We can calculate the upper limit of the crystallinity of the sandwich lamella model. Let the lamellae thickness be $(M_c + 2M_e)$-mer, where the thicknesses of the core and the edge are M_c-mer and M_e-mer, respectively. The fractional population of $(M_c + 2M_e)$-mer of which the central M_c-mer is composed of only HB units and the two terminal M_e-mers are arbitrary sequences is (1

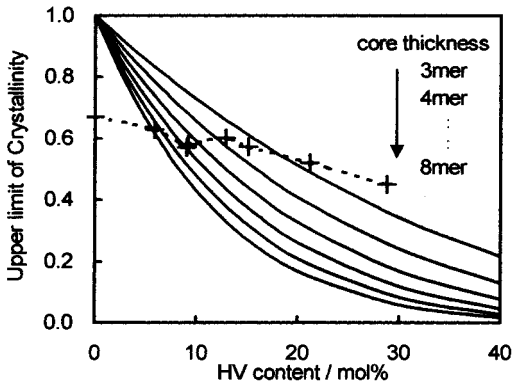

Figure 11. Upper limits of crystallinity allowed for copolymers forming sandwich lamella with the core of 3- to 8-mer thick. The crystallinity determined by WAXD is also plotted (cross).

$- f_{HV})^{M_c}$, where f^c_{HV} is the HV content in the crystalline phase. That is to say, the upper limit of the crystallinity (mole fraction) is $(1 - f_{HV})^{M_c}$. The relation between the upper limit of the crystallinity and the HV content for the sandwich lamella state with various core thicknesses is shown in Figure 11. It is clearly shown that as the thickness of the core increases and as the HV content increases, the upper limit of the crystallinity significantly decreases.

In this figure, the degree of crystallinity, χ_{waxd}, of the samples is also shown. Though χ_{waxd} is not exactly equal to the mole fraction of crystallinity, the difference between then is small compared with the experimental errors of χ_{waxd}. The data in Figure 11 show that the observed crystallinities, χ_{waxd}, of P(HB-*co*-6% HV) and P(HB-*co*-9% HV) can be realized by the sandwich lamella model only when the core thicknesses are shorter than 7-mer and 5-mer, respectively. Since the lamella thicknesses of P(HB-*co*-6% HV) and P(HB-*co*-9% HV) determined from SAXS (see Figure 5) correspond to 17-mer (=8.5 fiber periods) and 15-mer (=7.5 fiber periods), respectively, the lower limits of the edge thickness of both the samples are estimated to be 5-mer (=2.5 fiber periods). Thus, the HV units intrude into the lamella up to 2.5 periods from the surface. This suggests that the distortion of the PHB crystalline lattice by the HV units can be easily relaxed up to this depth. The similarity of the estimated thickness of the edge between P(HB-*co*-6% HV) and P(HB-*co*-9% HV) implies the suitability of the sandwich lamella model for describing the cocrystals of these copolymers.

The discussion above is on the structure of the P(HB-*co*-HV) copolymers crystallized at 90 °C. A logical consideration gives an idea that the possible structural transition may appear at different HV content depending on the crystallization conditions. Between the two models proposed here, the sandwich lamella must be closer to equilibrium. Therefore, the structural transition may appear at higher HV content for the copolymers crystallized at higher temperature. However, Figure 1b shows that the discontinuity in growth rate appeared at similar composition for the samples crystallized any temperature between 60 and 110 °C. This means that the crystallization condition give little influence on the possible structural transition. Figure 11 shows that, for P(HB-*co*-HV) containing more than 13 mol % HV, the sandwich lamella state with ca. 60% crystallinity can be realized only when the core is thinner than 3-mer. As mentioned above, the formation of such a thin core will give less advantage over the formation of uniform lamella. This explains why P(HB-*co*-HV) containing 13 mol % HV forms uniform lamella. Therefore, a structural transition from the sandwich lamella to the uniform lamella must be occur at a HV content lower than ca. 10 mol % independent of the crystallization condition. The results shown here are not enough to make further discussion and reach an accurate conclusion on the effect of the crystallization condition on the structure. We are now planning to investigate the samples crystallized at various temperatures systematically.

Conclusion

In this study, the structure of the isomorphous crystals of P(HB-*co*-HV) in the PHB crystalline lattice is examined in detail. It has been shown that the composition dependence of spherulite growth rate, crystallinity, lamella thickness, HV content in the crystalline phase, and melting temperature change discontinuously at ca. 10 mol % HV, implying the occurrence of a structural transition at this composition. We have introduced two models of lamellar crystals containing counits, i.e., sandwich lamella and uniform lamella, and have discussed the applicability of these models to the case of P(HB-*co*-HV). It has been concluded that these models consistently explain the results; the crystalline structures formed for HV content below and above 10 mol % can be described by the sandwich lamella and the uniform lamella, respectively. Though there had been many reports on the structure of P(HB-*co*-HV) and on the transition from the HB type crystal to the HV type crystal at ca. 50 mol % HV, none of them had mentioned a transition at ca. 10 mol % HV. This is probably because there were no reports on the investigation of a series of P(HB-*co*-HV) samples crystallized in the PHB crystalline lattice with well-combined analyses of X-ray, NMR, DSC, and polarized microscopy.

As is well-known, the nature of polymer crystals is strongly affected by kinetics. In the case of copolymer crystals, lamella thickness and composition in the crystalline phase are also controlled by kinetics.[28−30] The mechanism of the kinetic control will be discussed in a separate paper.[31]

Acknowledgment. The authors thank Prof. Asai of Tokyo Institute of Technology for his help with the WAXD and SAXS measurements. This work is partially supported by a Grant-in-Aid for Scientific Research on Priority Area, “Sustainable Biodegradable Plastics”, No. 11217205 (2001) from the Ministry of Education, Science, Sports and Culture (Japan).

References and Notes

(1) Sanchez, I. C.; Eby, R. K. *Macromolecules* **1975**, *8*, 638.
(2) Bluhm, T. L.; Hamer, G. K.; Marchessault, R. H.; Fyfe, C. A.; Veregin, R. P. *Macromolecules* **1986**, *19*, 2871.
(3) Kunioka, M.; Tamaki, A.; Doi, Y. *Macromolecules* **1989**, *22*, 694.
(4) Scandola, M.; Ceccorulli, G.; Pizzoli, M.; Gazzano, M. *Macromolecules* **1992**, *25*, 1405.
(5) Yamada, S.; Wang, L.; Asakawa, N.; Yoshie, N.; Inoue, Y. *Macromolecules* **2001**, *34*, 4659.
(6) Kamiya, N.; Sakurai, M.; Inoue, Y.; Chûjô, R. *Macromolecules* **1991**, *24*, 2178.
(7) VanderHart, D. L.; Orts, W. J.; Marchessault, R. H. *Macromolecules* **1995**, *28*, 6394.
(8) Sanchez-Cuesta, M.; Martinez-Salazar, J.; Barker, P. A.; Barham, P. J. *J. Mater. Sci.* **1992**, *27*, 5335.

(9) Barker, P. A.; Barham, P. J.; Martinez-Salazar, J. *Polymer* **1997**, *38*, 913.
(10) Barker, P. A.; Mason, F.; Barham, P. J. *J. Mater. Sci.* **1990**, *25*, 1952.
(11) Yoshie, N.; Sakurai, M.; Inoue, Y.; Chûjô, R. *Macromolecules* **1992**, *25*, 2046.
(12) Barker, P. A.; Barham, P. J.; Martinez-Salazar, J. *Polymer* **1997**, *38*, 913.
(13) Doi, Y.; Kunioka, M.; Nakamura, Y.; Soga, K. *Macromolecules* **1987**, *20*, 2988.
(14) Yoshie, N.; Menju, H.; Sato, H.; Inoue, Y. *Macromolecules* **1995**, *28*, 6516.
(15) Cao, A.; Kasuya, K.; Abe, H.; Doi, Y.; Inoue, Y. *Polymer* **1998**, *39*, 4801.
(16) Yoshie, N.: Inoue, Y. *Int. J. Biol. Macromol.* **1999**, *25*, 193.
(17) Kunioka, M.; Doi, Y. *Macromolecules* **1990**, *23*, 1933.
(18) Saito, M.; Inoue, Y.; Yoshie, N. *Polymer* **2001**, *42*, 5573.
(19) Bauer, H.; Owen, A. J. *Colloid Polym. Sci.* **1988**, *266*, 241.
(20) Hoffman, J. D. *Polymer* **1983**, *24*, 3.
(21) Yokouchi, M.; Chatani, Y.; Tadokoro, H.; Teranishi, K.; Tani, H. *Polymer* **1973**, *14*, 267.
(22) Cornibert, J.; Marchessault, R. H. *J. Mol. Biol.* **1972**, *71*, 735.
(23) Bloembergen, S.; Holden, D. A.; Hamer, G. K.; Bluhm, T. L.; Marchessault, R. H. *Macromolecules* **1986**, *19*, 2865.
(24) Sánchez, M.; Martínez-Salazar, J.; Barker, P. A.; Barham, P. J. *J. Mater. Sci.* **1992**, *27*, 5335.
(25) Mitomo, H.; Morishita, N.; Doi, Y. *Polymer* **1995**, *36*, 2573.
(26) Orts, W. J.; Marchessault, R. H.; Bluhm, T. L. *Macromolecules* **1991**, *24*, 6435.
(27) Abe, H.; Doi, Y.; Aoki, H.; Akehata, T. *Macromolecules* **1998**, *31*, 1791.
(28) Helfand, E.; Lauritzen, Jr., J. I. *Macromolecules* **1973**, *6*, 631.
(29) Kamiya, N.; Sakurai, M.; Inoue, Y.; Chûjô, R. *Macromolecules* **1991**, *24*, 3888.
(30) Barham, P. J.; Barker, P. A.; Organ, S. J. *FEMB Microbiol. Rev.* **1992**, *103*, 289.
(31) Yoshie, N.; Yazawa, K.; Inoue, Y. Manuscript in preparation.

MA0113071